Surface & Coatings Technology 217 (2013) 124–128

Contents lists available at SciVerse ScienceDirect

Surface & Coatings Technology

journal homepage: www.elsevier.com/locate/surfcoat

Thermographic analysis and modelling of the delamination crack growth in a thermal barrier coating on Fecralloy substrate

Mario Schweda *, Tilmann Beck, Marita Offermann, Lorenz Singheiser

Research Centre Jülich GmbH, IEK-2, 52425 Jülich, Germany

ARTICLE INFO

Article history:
Received 22 February 2012
Accepted in revised form 4 December 2012
Available online 13 December 2012

Keywords:
Thermal barrier coating (TBC)
Crack growth
Delamination
Thermography
Modelling
Lifetime

ABSTRACT

The delamination crack growth in a plasma sprayed ZrO_2 thermal barrier coating system during thermal cycling was analysed by thermography. A simplified model system was used where a Fe–Cr–Al–Y alloy (Fecralloy Eisen-Chrom ™) substrate with relative low yield stress and creep strength simulates the bond coat. The delamination crack area was measured as a function of cycle number and the growth mechanisms were observed and quantified by infrared pulse thermography. Based on this, an empirical model was created to describe the delamination crack growth. In contrast to most of the usual models, the present model calculates delamination crack area (instead of length), accounts for formation of multiple cracks (instead of one), for crack initiation at different times (instead simultaneous initiation), for the positions of the cracks on the sample and to each other as well as for the statistic spatial distribution of the crack initiation sites. The key features of delamination crack growth are met properly by the model approach. Although only one set of parameters was used, the model captures temporal discontinuities of the crack area increase and therefore scatter of delaminated area at a given time.

1. Introduction

Thermal barrier coatings (TBCs) are applied on gas turbine components, especially blades and vanes in the first turbine stages made of Ni-superalloy, to protect them from heat and corrosion. The TBC consists of partially Y_2O_3 stabilised ZrO_2 (P-YSZ) deposited by air plasma spraying (APS) or electron beam physical vapour deposition (EBPVD). A Ni(Co) CrAlY bondcoat (BC) under the TBC ensures sufficient adhesion to the substrate and protects the substrate from oxidation by forming a dense Al_2O_3 scale (thermally grown oxide — TGO). In case of plasma sprayed TBC systems, the BC is additionally roughened by sand blasting to ensure mechanical bonding of the TBC. The BC is usually deposited by vacuum plasma spraying (VPS) [1–3].

During operation of the turbine stresses arise in the coating system, caused by thermal expansion mismatch of its components during heating and cooling, by sintering of the TBC as well as by the orthogonal and lateral TGO growth at high temperature [4–8]. As soon as these stresses, which are partially accommodated by creep processes, exceed a critical value, cracks form, mainly in the TBC–BC interface. Their coalescence finally leads to delamination and spallation of the TBC.

To prevent subsequent damage by spalled TBC, the coated parts have to be revised in certain intervals before spallation becomes probable. Therefore, reliable life prediction models need to be developed. For example Miller, DeMasi and others created empirical formulas, which correlate the cycles to failure with the inelastic strain range of the TBC-system and the oxide growth [9,10]. Other authors created models using fracture mechanics approaches where the system is reduced to 2 dimensions: Hutchinson et al. proposed models which deal with delamination crack growth and TBC-buckling at ideally flat TBC–BC-interfaces [11]. Beck, Vaßen, Traeger, Aktaa and others created models calculating crack initiation and subsequent crack growth at rough TBC–BC-interfaces by fracture mechanics [12–15]. Stresses are determined analytically by physics-based or empirical functions or by finite element method (FEM). Crack growth is assumed to be proportional to the TGO-thickness (in the initiation phase) or calculated as a function of energy release rate G or stress intensity factor K. Seiler, Bialas and others simulated crack propagation at a rough TBC–BC-interface by FEM also using the energy release rate G [16,17]. To limit calculation complexity in the models of Beck, Vaßen, Traeger, Aktaa, Bialas and Seiler a periodic interface roughness is assumed. Those models are restricted to the simulation of only one crack or of simultaneous crack initiation and growth at every roughness period and to calculation of crack length in a 2-dimensional configuration. FEM-simulations of Bäker, Bednarz, Busso, Aktaa and others showed that the stress level at a single roughness peak strongly depends on the amplitude and shape of the roughness profile [5,6,13,18]. Therefore, in real TBC-systems with stochastic roughness distribution, the critical stress for crack nucleation is reached at different roughness peaks at different times. This suggests a progressive nucleation and growth of delamination zones in real systems, which has been proved experimentally in [19]. Hille [20,21] and Busso [18] published models which account for the initiation of multiple cracks at different times. Hille made

* Corresponding author at: Forschungszentrum Jülich GmbH, IEK-2, 52425 Jülich, Germany. Tel.: +49 2461 615096; fax: +49 2461 618293.
E-mail address: m.schweda@fz-juelich.de (M. Schweda).

0257-8972
http://dx.doi.org/10.1016/j.surfcoat.2012.12.002

FEM-simulations of stresses in TBC-systems with a rough TBC–BC-interface (taking into account the TGO-growth as well as visco-plastic behaviour of the BC) and simulated crack nucleation and propagation using cohesive zone elements. Busso correlated measured total TBC damage as a function of accumulated time at high temperature with measured TBC–BC-interface roughness depth distribution. However, Hille's and Busso's models do not account for the statistic spatial distribution of the crack initiation sites over the sample surface.

In the present study TBC-coated samples were thermally cycled and the delamination crack growth was observed by thermography. The delaminated area was measured as a function of thermal cycle number and the formation and growth kinetics of delamination cracks were quantified by thermography. Based on this, an empirical model was created to describe the delamination crack growth. This model is not based on fracture mechanics, but it calculates – in contrast to other models – crack area (instead of length), accounts for formation of multiple delamination cracks (instead of one), for crack initiation at different times (instead simultaneous initiation), for the positions of the cracks on the sample and to each other as well as for the statistical spatial distribution of the crack initiation sites.

2. Test material and experimental procedure

A simplified model TBC system was produced: to exclude the influence of thermal mismatch and interdiffusion between Ni-superalloy and bond coat, the iron base alloy "Fecralloy Eisen-Chrom", which has similar oxidation kinetics and thermal expansion coefficient as typical bondcoat alloys, was used as substrate. However, Fecralloy has a lower yield stress and creep strength than usual Ni(Co)CrAlY-bondcoats [22–24]. Fecralloy was delivered by GoodFellow as rod with 74.0 wt.% Fe, 4.84 wt.% Al, 21.8 wt.% Cr and <0.005 wt.% Y.

Cylindrical specimens with a length of 30 mm and a diameter of 9 mm were produced by turning. The substrates were roughened by sand blasting at Technische Universität Braunschweig, IfW. Finally, an 8% Y_2O_3 partially stabilised APS–ZrO_2–TBC was deposited at Technische Universität Braunschweig, IfW, with a coating thickness of 300 μm and tapered edges.

The samples were thermally cycled by moving them automatically into and out of a tube furnace. The minimum and maximum temperatures were 60 °C and 1050 °C, respectively. The dwell time at maximum temperature was 2 h and the heating and cooling time 13.3 min, each. Further details of the specimen preparation and thermal cycling are given in [19].

The damage evolution was documented by thermography. Therefore, the samples were removed from the furnace in intervals of approximately 9 cycles and cooled to room temperature. An infrared camera was used (FLIR, ThermaCam2000, quantum well infrared photon detector (QWIP), resolution of 320×240 pixels, spectral range of 8–9 μm, thermal sensitivity of 20 mK at 30 °C, absolute accuracy of ±1 °C up to 150 °C, maximum sampling frequency of 50 Hz, objective 20°×15°/0.3 m, 106 μm close-up lens 34 mm×25 mm/100 mm). A heat pulse with a duration of 0.01 s was imposed to the samples using two flash light bulbs directed perpendicular to the longitudinal axis of the test pieces and arranged at an angle of ±45° with respect to the optical axis of the infrared camera. The surface temperature of the specimen reaches a maximum at 0.04 s after the heat pulse and subsequently decreases. During the temperature increase and the cooling phase, 20 temperature images were made with a sampling frequency of 50 Hz. To enable the comparison of measurements with different initial temperature distributions (before the temperature increase), the initial temperature distribution was subtracted from the temperature distribution in all following thermographic images. Finally the temperature distributions were normalised, by dividing them by the temperature distribution at 0.04 s after the heat pulse (where the peak temperatures were measured). In the delaminated regions the heat flux is decreased, resulting in increased temperature during cooling compared with the undelaminated regions. For evaluation of the delaminated zones the image at 0.08 s after the heat pulse start was used. An effect of microstructural changes in the TBC, e.g. induced by sintering during thermal exposure, on the surface temperature in the undelaminated zones was not observed. Each sample was analysed from 4 sides by turning the sample through 90° around its longitudinal axis to obtain data from the whole surface. Greenish thermography areas represent adherent TBC, yellow and red zones indicate delamination of the TBC (see Figs. 1 and 2). Cernuschi et al. [25] state that small, early-stage delamination cracks cannot be clearly identified by non-destructive evaluation techniques (IR thermography and other methods). Accordingly, the detection limit of the thermography analysis conducted in the present study was evaluated carefully at metallographic cross sections through the smallest features indicating delaminations in thermography, proving that delaminations up from a diameter of 0.7 mm and a TBC lift-off of 2 μm could be clearly identified by thermography (see Fig. 1).

The delaminated area was measured from the thermographies using the phase measuring tool of the software analySIS. Therefore regions with RGB colour space coordinates of R = 255, G = 0–255 and B = 0–255 were defined as delaminated zones and adherent otherwise. Although the substrate roughness depth was varied by sand blasting with four different grain sizes (0–50, 60–120, 150–250 and 355–600 μm) and some samples were pre-oxidised at 1050 °C for 220 h in air (resulting in an initial TGO thickness of averaged 2.4 μm) this had no significant influence on the damage evolution [19]. Therefore, these results will be considered to be equivalent in the following sections.

3. Results and discussion

3.1. Thermography

The total delamination crack area on one single sample side was measured from the thermographies as a function of cycle number for all samples. The delamination area usually increases relatively slowly with increasing cycle number. In some cases discontinuities are observed where the growth rate is temporally higher, resulting in a relative strong scatter of delaminated area at a given time. However, the fundamental damage evolution process observed by thermography is similar for all specimens. A typical series of thermography images is shown in Fig. 2. There is an incubation time during which no delaminations are detected in the thermography images. Afterwards, circular delaminations with an average diameter of 0.7 mm occur, which we call "initial delaminations" (ID). The average ID-diameter corresponds to a delamination area of 0.38 mm^2, which we call initial ID-area A^*. During

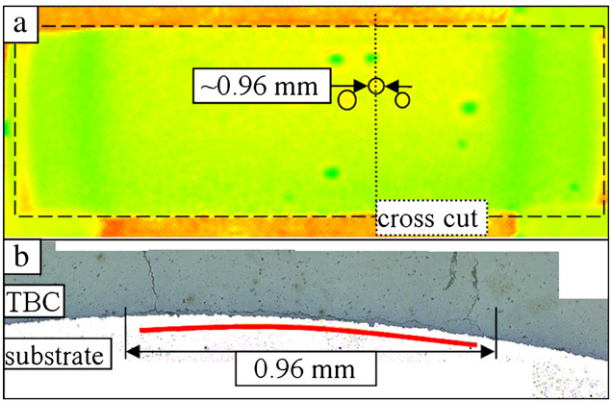

Fig. 1. a) Thermography image of one sample side with yellow zones (the sample size is given by a dashed line, the red border represents the background that is the table on which the samples were placed, the yellow zones are indicated by black circles) and b) cross section through one of these yellow zones.

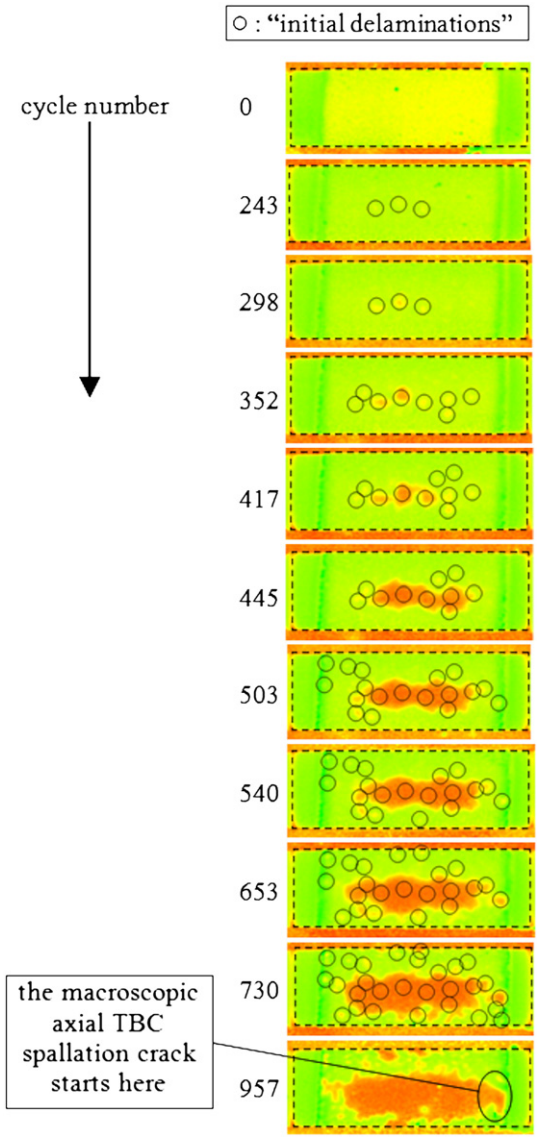

Fig. 2. Typical thermography image series of one sample side. The sample size is given by a dashed line. The red border represents the background that is the table on which the samples were placed. Initial delaminations are indicated by black circles. Note that circles which lay on continuous delamination strips, indicate initial delaminations which occurred before the strip formation.

further cycling the number and size of the IDs increase and they link together, forming larger delamination blisters which grow further. New IDs form preferred in the vicinity of existing IDs in the axial direction of the sample. Thus, a longitudinal "strip-like" delamination area forms during further thermal cycling. As soon as the delamination strip enters the tapered edge of the TBC and reaches a certain size, the delamination becomes visible by lift-off of the TBC at this location. The macroscopic axial TBC-segmentation crack which finally causes spallation of the TBC typically initiates there.

In order to develop an appropriate modelling approach describing the delamination crack growth, the damage evolution observed by thermography was studied in more detail and quantified: the incubation time, which we call N_{In}, i.e. the cycle number after which the first ID occurs, was determined for several tested samples. The median incubation time is 48 cycles (measured at 44 samples, average of 63.8 cycles, standard deviation of 60.1 cycles). Furthermore, the total number of IDs was counted and the size of single IDs (until they link together with other delaminations) was measured as a function of thermal cycle number for several samples. Both, the number and the individual size of IDs increase nearly linearly with the cycle number. The ID formation rate (which we call ΔN) and the ID growth rate (which we call v) were calculated by linear approximation. The median of the formation rates is 18 cycles (measured at 10 samples, average of 18.3 cycles, standard deviation of 7.0 cycles). The median of the growth rates is 2630 μm^2/cycle (measured at 15 samples, average of 3682 μm^2/cycle, standard deviation of 2604 μm^2/cycle).

As mentioned above, new IDs form preferred in the vicinity of existing IDs in axial direction of the sample. To quantify this behaviour, the "delamination group" was defined as the smallest rectangle on one thermography image which encloses all delaminations. The size of a "delamination group" in axial direction of the sample is called "length" and the size in circumferential direction is called "width". Length and width were measured as a function of thermal cycle number at different samples. The growth rates were determined by linear approximation. The length of the delamination groups increases 3–9 times faster during thermal cycling than their width (measured at 3 samples).

3.2. Modelling

Based on the delamination growth mechanisms explained above, a programme was written using the software Scilab version 5.2.1 to simulate the delamination area growth as a function of thermal cycle number N: A field was defined with the dimensions of the projected area of the experimentally tested samples (9 mm × 30 mm). Inside this field initial delaminations (IDs, as defined in Section 3.1) are generated in form of circles with initial diameters of 0.7 mm (area of $A^* = 0.38$ mm^2). With increasing cycle number these IDs grow and coalesce. According to the experimental findings in Section 3.1 the number of IDs and the area of single IDs are assumed to increase linearly with increasing thermal cycle number. A constant incubation time of $N_{In} = 48$ cycles, a constant ID formation rate of $\Delta N = 18$ cycles and a constant ID growth rate of $v = 2630$ μm^2/cycle was chosen (medians of the determined values — see Section 3.1). The preferred formation of IDs in the vicinity of the existing delaminations (see Fig. 2) and the faster growth of the "delamination group" in axial sample direction were included in the model by restricting the ID-generation to the interior of rectangles whose size in axial sample direction increase faster than in circumferential direction. The formation of two delamination groups on the considered surface area was allowed. The following formalism was used:

1 At cycle N_{In} and $N_{In} + \Delta N$ the first two circular IDs are generated at random positions, both with an initial area of A^*. These IDs are the origins of the two possible delamination groups.
2 The growth of a delamination group in axial direction was, according to the experimental observations, chosen to be 6 times faster than in circumferential direction (the average of the determined values): in each step of ΔN cycles two rectangles are created that exactly enclose the centre points of all IDs within each delamination group. Then both rectangles are enlarged in axial sample direction by adding 6 times the radius of the largest ID inside the rectangle at both rectangle sides and in the circumferential direction by adding 1 time the radius.
3 One new ID is generated in steps of $\Delta N = 18$ cycles inside one of these rectangles.
4 Steps 2 and 3 are repeated until the simulation is stopped.

Fig. 3 shows an example of a simulation after different cycle numbers. The total delaminated area was determined by calculating the total circle-area (as a lower margin of the delaminated area) and the total area surrounded by the rectangles (as upper margin) as a function of thermal cycle number without double-counting of overlapping. A set of calculated delamination crack growth curves, representing both, the area sum of the circles and of the rectangles, is shown in Fig. 4 together with experimentally obtained delamination growth curves. The simulated and experimental data lie in the same range and the most experimental results are

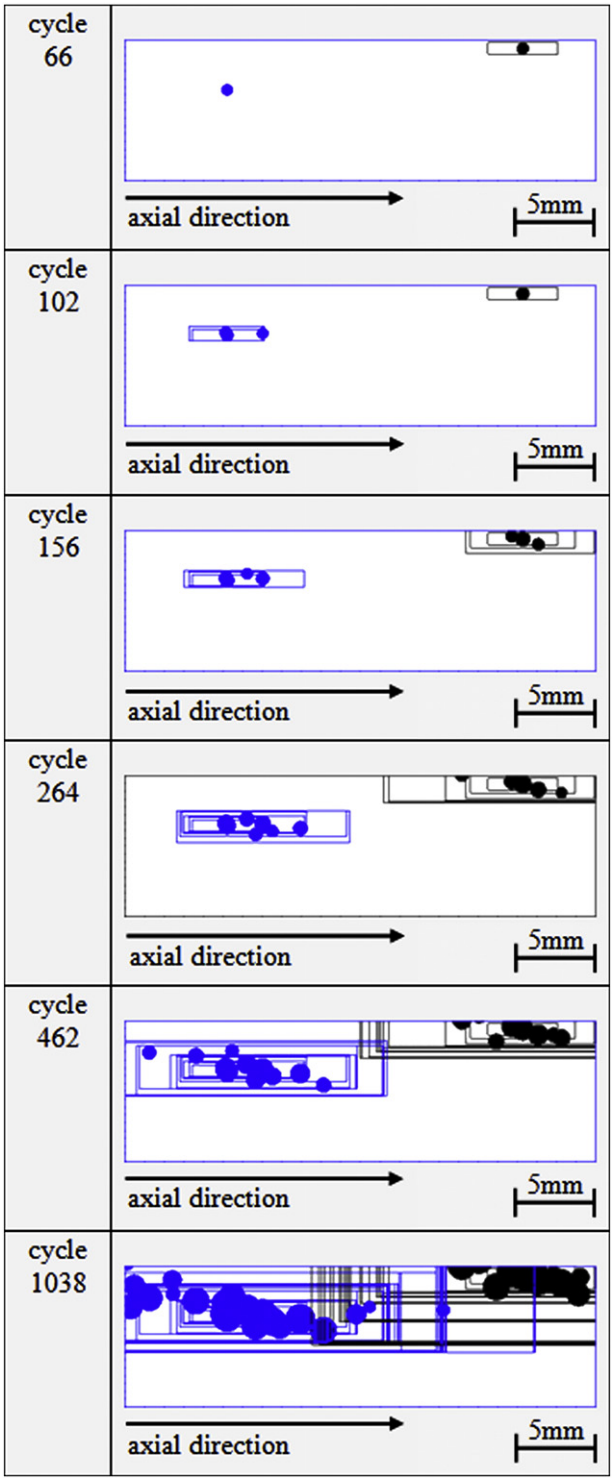

Fig. 3. Simulation of the delamination area growth according to the model after different cycle numbers.

enclosed by the upper and lower margins of the calculated delamination area. It should be noted that all calculations were performed using the median values of incubation time, ID formation rate and ID growth rate. Accordingly, the scatter of the experimental crack growth curves is reflected in the model only by random choice of the ID positions, first on the complete sample surface and afterwards within the delamination groups as well as by subsequent interaction of growing delaminations which in turn depends on the randomly chosen ID positions. Interestingly this relatively simple model approach also captures sudden changes of the delamination growth rate observed in most of the experiments by randomly choosing the ID position and assuming fixed values of incubation time, ID formation and growth rates. This proves that the key features of delamination growth observed in the experiments, namely (i) linear ID formation rate, (ii) linear area growth rate of existing delaminations and (iii) preferred formation of new IDs in a defined vicinity of existing delaminations, are sufficient to describe the whole TBC degradation process quantitatively.

4. Conclusion and outlook

The delamination crack growth evolution of an APS–P-YSZ–TBC on Fe–Cr–Al–Y substrate during thermal cycling with 2 h high temperature dwell at a maximum temperature of 1050 °C was analysed by thermography (Fig. 2). The delamination crack growth was observed by infrared pulse thermography and the formation and growth of delaminated areas was quantified by image analysis. Based on this, an empirical model was created to describe the increase of delamination crack area (compare Fig. 3). The model is not based on fracture mechanics, but it calculates – in contrast to many other models – crack area (instead of length), account for the formation of multiple delamination cracks (instead of one) and for crack initiation at different times (instead of simultaneous initiation). Additionally, the model considers the statistical spatial distribution of the crack initiation sites and the positions of the cracks to each other. The following conclusions can be drawn:

- The model captures the experimentally observed scatter of the delaminated area vs. time although only one set of parameters (the medians of the experimental values of incubation time, ID formation and growth rate and the average ratios of the growth rates of the delamination groups width and length) is used (Fig. 4).
- The model also captures temporal changes of the delamination growth rate observed in most of the experiments (Fig. 4).
- The fact that the modelled and experimentally obtained delamination growth data (including their considerable scatter) agree well (Fig. 4), indicates that the key features of delamination crack initiation and propagation are met properly by the model approach.

Since the used TBC-system is a model system, the transferability of the delamination growth model to real TBC systems will be investigated in future. A second challenge is to connect the model with physical aspects like interfacial strength, toughness and roughness, mechanical stresses and specimen geometry. For example the crack initiation sites could be determined by calculating the positions of critical stress from a measured roughness distribution.

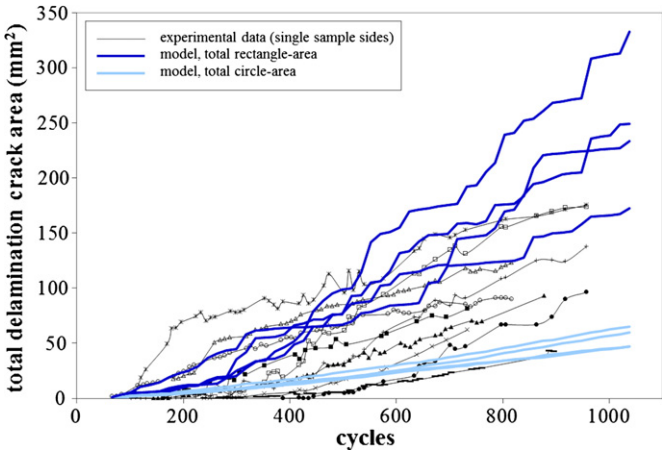

Fig. 4. Total delamination crack area on one sample side as a function of cycle number, experimentally measured and modelled.

Acknowledgement

This work was financially supported by the German Research Association (DFG).

References

[1] N.P. Padture, M. Gell, E.H. Jordan, Science 296 (2002) 280.
[2] N.S. Cheruvu, K.S. Chan, R. Viswanathan, Mater. Sci.Eng. Energy Syst. 1–1 (March 2006) 33.
[3] J. DeMasi–Marcin, D.K. Gupta, Surf. Coat. Technol. 68/69 (1994) 1.
[4] J. Rösler, M. Bäker, K. Aufzug, Acta Mater. 52 (2004) 4809.
[5] M. Bäker, J. Rösler, G. Heinze, Acta Mater. 53 (2005) 469.
[6] P. Bednarz, Finite element simulation of stress evolution in thermal barrier coating systems, Dissertation RWTH Aachen, 2006.
[7] R.V. Hillery, B.H. Pilsner, R.L. McKnight, in: National Aeronautics and Space Administration, 1988.
[8] R.A. Miller, Surf. Coat. Technol. 30 (1987) 1.
[9] J.T. DeMasi, K.D. Sheffler, M. Ortiz, NASA Contractor Report 182230, National Aeronautics and Space Administration, 1989.
[10] R.A. Miller, J. Am. Ceram. Soc. 67–8 (1984) 517.
[11] J.W. Hutchinson, Z. Suo, in: J.W. Hutchinson, T.Y. Wu (Eds.), Advances in Applied Mechanics, vol. 29, Academic Press, Inc., Boston, 1992, p. 63.
[12] T. Beck, R. Herzog, O. Trunova, M. Offermann, R.W. Steinbrech, L. Singheiser, Surf. Coat. Technol. 202 (2008) 5901.
[13] J. Aktaa, K. Sfar, D. Munz, Acta Mater. 53 (2005) 4399.
[14] R. Vaßen, G. Kerkhoff, D. Stöver, Mater. Sci. Eng. A303 (2001) 100.
[15] F. Traeger, M. Ahrens, R. Vaßen, D. Stöver, Mater. Sci. Eng. A358 (2003) 255.
[16] M. Bialas, P. Bednarz, R. Herzog, in: J. Lecomte-Beckers, M. Carton, F. Schubert, P.J. Ennis (Eds.), Materials for Advanced Power Engineering 2006, Proceedings of the 8th Liège Conference Part II, Schriften des Forschungszentrums Jülich, Reihe Energietechnik, vol. 53, 2006, p. 747.
[17] P. Seiler, M. Bäker, J. Rösler, IOP Conf. Ser.: Mater. Sci. Eng. 10 (2010) 012056.
[18] E.P. Busso, L. Wright, H.E. Evans, L.N. McCartney, S.R.J. Saunders, Acta Mater. 55 (2007) 1491.
[19] M. Schweda, T. Beck, L. Singheiser, Int. J. Mater. Res. 103 (2012) 40.
[20] T.S. Hille, T.J. Nijdam, A.S.J. Suiker, S. Turteltaub, W.G. Sloof, Acta Mater. 57 (2009) 2624.
[21] T.S. Hille, S. Turteltaub, A.S.J. Suiker, Eng. Fract. Mech. 78 (2011) 2139.
[22] M. Schweda, Optimierung von APS-ZrO2-Wärmedämmschichten durch Variation der Kriechfestigkeit und Grenzflächenrauhigkeit, Dissertation RWTH Aachen, 2010.
[23] S. Heckmann: Ermittlung des Verformungs- und Schädigungsverhaltens von Wärmedämmschichtsystemen, Dissertation RWTH Aachen (2003).
[24] M.G. Hebsur, R.V. Miner, Mater. Sci. Eng. 83 (1986) 239.
[25] F. Cernuschi, S. Capelli, P. Bison, S. Marinetti, L. Lorenzoni, E. Campagnoli, C. Giolli, Acta. Mater. 59 (2011) 6351.